Song *et al.*
Chinese Journal of Mechanical Engineering (2023) 36:154
https://doi.org/10.1186/s10033-023-00977-4

Chinese Journal of Mechanical Engineering

ORIGINAL ARTICLE

Open Access

Configuration Design and Kinematic Performance Analysis of a Novel 4-DOF Parallel Ankle Rehabilitation Mechanism with Two Virtual Motion Centers

Jingke Song[1,2,3], Jun Wei[1,2,3], Bin Yu[1,2,3], Chenglei Liu[1,2,3], Cunjin Ai[1,2,3] and Jianjun Zhang[1,2,3*]

Abstract

Aiming at the problem that the existing ankle rehabilitation robot is difficult to fully fit the complex motion of human ankle joint and has poor human-machine motion compatibility, an equivalent series mechanism model that is highly matched with the actual bone structure of the human ankle joint is proposed and mapped into a parallel rehabilitation mechanism. The parallel rehabilitation mechanism has two virtual motion centers (VMCs), which can simulate the complex motion of the ankle joint, adapt to the individual differences of various patients, and can meet the rehabilitation needs of both left and right feet of patients. Firstly, based on the motion properties and physiological structure of the human ankle joint, the mapping relationship between the rehabilitation mechanism and ankle joint is determined, and the series equivalent model of the ankle joint is established. According to the kinematic and constraint properties of the ankle equivalent model, the configuration design of the parallel ankle rehabilitation robot is carried out. Secondly, according to the intersecting motion planes theory, the full-cycle mobility of the mechanism is proved, and the continuous axis of the mechanism is judged based on the constraint power and its derivative. Then, the kinematics of the parallel ankle rehabilitation robot is analyzed. Finally, based on the OpenSim biomechanical software, a human-machine coupling rehabilitation simulation model is established to evaluate the rehabilitation effect, which lays the foundation for the formulation of a rehabilitation strategy for the later prototype.

Keywords Ankle rehabilitation robot, Double-VMCs mechanism, Kinematic performance, Human-machine rehabilitation simulation

1 Introduction

The ankle joint is a complex joint of the lower limbs, which is closely linked by ligaments and muscles, and plays a role in maintaining human body balance and providing power for walking in daily life [1]. The ankle joint is also one of the most vulnerable joints in the human body, there are two main causes for its injury: one is the joint sprain caused by external force in daily life, and the other is the ankle function injury caused by neurological diseases, such as stroke, spinal cord injury and other diseases [2, 3]. There are about 15 million people worldwide who suffer from stroke every year [4], including 795000 stroke patients in the United States every year. According to the prediction by the American Heart Association, the number of stroke patients will rise to 3.4 million by 2030 [5].

*Correspondence:
Jianjun Zhang
zhjjun@hebut.edu.cn
[1] School of Mechanical Engineering, Hebei University of Technology, Tianjin 300401, China
[2] Hebei Provincial Key Laboratory of Robot Perception and Human-Machine Fusion, Tianjin 300130, China
[3] Intelligent Rehabilitation Device and Detection Technology Engineering Research Center of the Ministry of Education, Tianjin 300130, China

Traditional ankle rehabilitation therapy relies on manual assistance from doctors to help patients perform dorsiflexion/plantar flexion, inversion/eversion, and other movements. The goal is to gradually stimulate and repair the damaged central nervous system of the ankle. However, this rehabilitation process is time-consuming and repetitive, placing a significant burden on therapists [6]. Due to the imbalance in the doctor-patient ratio and the limitation of therapy time and resources, it is difficult for traditional ankle rehabilitation to ensure sufficient therapy frequency and intensity [7]. Therefore, the development of an ankle rehabilitation robot to replace traditional artificial rehabilitation therapy meets the market demand and is of great significance.

The series mechanism has limitations due to the motor's inability to be completely fixed, increased motion inertia, and difficulty in fitting within a smaller ankle space. In contrast, the parallel mechanism (PMs) has the advantages of smaller accumulative error, higher precision, larger loading capacity, easy closed-loop control, and stable motion [8]. Therefore, many scholars have extensively researched and designed ankle rehabilitation robots based on parallel mechanisms. Girone et al. [9] developed a 6-DOF ankle rehabilitation robot based on the Stewart platform, which can simulate the true motion of the ankle joint. However, it has drawbacks like redundant degrees of freedom, complex control, high cost, limited rotation space, and large space occupation. To address these issues, some scholars simplified the ankle joint as a 2-DOF universal (U) joint or a 3-DOF spherical (S) joint. They designed 2-DOF or 3-DOF parallel ankle rehabilitation robots with the unconstrained branch as the driving branch and the universal or spherical joint as the constraint branch. For example, Dai et al. [10] developed a high-performance 3-UPS/U ankle rehabilitation robot with two rotational degrees of freedom, which can achieve ankle dorsiflexion, plantar flexion, inversion, and eversion movement. Similarly, there are 3-SPS/S [11] and 3-RSS/S [12] ankle rehabilitation robots with three rotational DOFs. The ankle rehabilitation mechanism has the advantages of simple structure, good kinematic performance, small space occupation and relatively low cost. However, these rehabilitation robots have their limitations. The motion center of these robots does not align with the center of the human ankle joint, which can potentially cause secondary injuries. Additionally, the rotation space is constrained by the middle spherical joint's rotation angle.

In order to solve the problem that the rotation center of the robot does not match the center of the human ankle joint, some scholars replace U or S joints with RR or RRR branches, such as Fang et al. [13] proposed a 3-RUS/RRR parallel mechanism and designed it as an ankle rehabilitation robot. Li et al. [14] proposed a 2-UPS/RRR ankle rehabilitation robot with three rotational DOFs, which has good kinematic performance and can complete active and passive rehabilitation therapy. Some scholars have designed a series of ankle rehabilitation mechanisms [15, 16] with the remote center of motion (RCM) [17], ensuring alignment between the human ankle center and the virtual rotation center of the mechanism. For example, Malosio et al. [18] designed an ankle rehabilitation robot based on the 3-RRR spherical robot (Agile eye). This robot features a relatively complex structure and an RCM, offering a favorable rehabilitation treatment effect on the ankle as the ankle center remains close to the motion center of the mechanism.

The ankle joint consists of the tibiotalar joint and subtalar joint, which have non-intersecting axes and a spatial interfacial relationship. However, the aforementioned scholars consider the ankle joint as an S joint or U joint with intersecting rotation axes, which deviates from the anatomical structure of the human ankle joint. This mismatch leads to a disparity between the actual motion of the rehabilitation robot and the ankle joint, resulting in poor coordination between human and machine motion. Moreover, the robot may exert non-DOF directional force on the human body, potentially causing secondary damage and negatively impacting rehabilitation outcomes and human comfort. Additionally, the differences in physiological structures among patients pose a challenge. The left and right feet have distinct anatomical characteristics, with opposite inclinations of the ankle axis. As a result, most ankle rehabilitation robots cannot accommodate the rehabilitation needs of both feet simultaneously. These factors emphasize the importance of developing ankle rehabilitation robots that accurately replicate the complex motion and spatial interfacial relationship of the human ankle joint while accommodating individual physiological differences between patients' left and right feet.

To address the aforementioned challenges, Liu et al. [19, 20] proposed a series of generalized spherical parallel ankle rehabilitation mechanisms based on the ankle bone structure. These mechanisms feature two rotational center points corresponding to the tibiotalar joint and subtalar joint centers. The distance between the two center points corresponds to the size of the talus of the ankle joint. The mobile platform of the mechanism allows rotation around these two center points individually or simultaneously, replicating the compound motion of the ankle joint more accurately and exhibiting promising rehabilitation potential. However, these mechanisms utilize multiple arc-shaped connecting rods, making the structure complex and requiring higher processing and installation accuracy. Moreover, during compound

motion of the ankle joint, the rotation axis of the mechanism changes with its pose variations. Consequently, it becomes challenging to ensure precise alignment between the mechanism's motion axis and the ankle joint's two rotation axes. While the mechanism aligns the rotation centers with the joint centers of the ankle, this limitation may still pose a risk of secondary damage to the ankle joint.

Therefore, this paper proposes a novel parallel ankle rehabilitation robot with three rotational and one translational (3R1T) DOF, taking into account the physiological and anatomical model of the human ankle joint. It features two virtual motion center (VMC) points and two rotation planes, enabling continuous rotation along specific lines without unintended motion. The VMC points correspond to the tibiotalar joint center and subtalar joint center. The distance between these points can be adjusted to accommodate different ankle heights. The robot also considers variations in deviation angles and inclination angles among patients. It offers benefits such as improved human-machine motion compatibility, suitability for diverse patients, easy wearing, and high safety.

In summary, the main work and innovation of this paper are as follows. Firstly, based on the motion properties and anatomical model of the human ankle joint, the mapping relationship between the ankle joint and the rehabilitation mechanism is determined. A novel equivalent model of the series ankle joint is proposed, which can provide guidance for the configuration design of the ankle rehabilitation robot. Secondly, a novel parallel mechanism with three rotational and one translational (3R1T) DOF is proposed. The mechanism has unique motion properties and has two virtual center points, which can realize fixed-point rotation around two virtual centers. This mechanism can be well applied in the field of ankle rehabilitation. Thirdly, according to the kinematic properties of the mechanism, it can be equivalent to a series branch chain. Combined with DH method, the inverse kinematics model of the rehabilitation mechanism can be easily established. Then, the inverse kinematics model, kinematic performance, and workspace of the mechanism are analyzed. Finally, based on the OpenSim biomechanical software, the human musculoskeletal model is coupled with the rehabilitation robot to establish a human-machine rehabilitation simulation model, and the evaluation index is defined to evaluate the rehabilitation effect.

The paper is organized as follows: In Section 2, considering the physiological anatomy model of the human ankle joint, a novel ankle rehabilitation robot is designed, and its mobility is analyzed based on screw theory. In Section 3, based on the intersection theory of the motion plane, the motion property and the full-cycle mobility of the mechanism are further distinguished, and the continuous axis of the mechanism is distinguished based on the constraint power and its derivative. In Section 4, according to the motion property of the mechanism, it can be equivalent to a series of branched chains, and the inverse kinematics model of the mechanism is established. In Section 5, given the size of the prototype, the kinematic performance of the rehabilitation mechanisms is discussed based on the motion/force transmission index and constraint index. Then, considering the singular configuration, driving stroke, and interference conditions of the mechanism, the workspace of the rehabilitation robot is analyzed. In Section 6, the human-machine rehabilitation simulation model is established to verify and evaluate the rehabilitation performance of the mechanism. Section 7 is the conclusion.

2 Configuration Design and Mobility Analysis of the Rehabilitation Mechanism

2.1 Establishment of Human Ankle Joint Equivalent Model

Understanding the biomechanical model of the human ankle joint is a prerequisite for ankle rehabilitation robot design. The ankle joint is divided into narrow concept ankle joint and generalized ankle joint. The narrow concept of the ankle joint only refers to the tibiotalar joint. The generalized ankle joint includes the tibiotalar joint, subtalar joint, and the talus between them. The ankle rehabilitation is mainly aimed at the generalized ankle joint. The anatomical structure of the ankle joint is very complex because it involves many components in a smaller space: four independent bones and many muscles and ligaments, as shown in Figure 1. The tibia is connected with the fibula and the upper surface of the talus to form the tibiotalar joint. The lower surface of the talus is connected with the upper surface of the calcaneus to form the subtalar joint. The ankle joint can be regarded

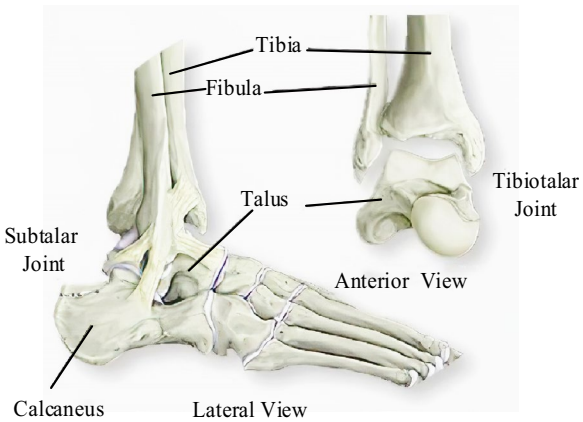

Figure 1 Physiological anatomy of the ankle [3]

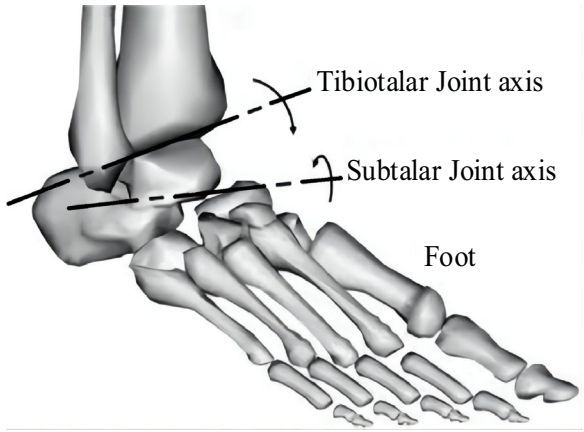

Figure 2 Ankle joint rotation axis diagram [21]

as a composite joint composed of the tibiotalar joint and the subtalar joint, as shown in Figure 2.

The axis of the tibiotalar joint, which plays a crucial role in ankle movement, can be defined as the line connecting the anterior edge of the lateral malleolus tip to the midpoint of the medial malleolus tip. However, it's important to note that the lateral malleolus extends significantly farther back than the medial malleolus, resulting in a complex orientation of the tibiotalar joint axis. This orientation includes both upward and downward inclinations, as well as left-right deviations. In general, it is widely accepted that the tibiotalar joint axis forms an angle of approximately 10° with the transverse plane and around 6° with the coronal plane [22]. However, it's worth mentioning that the specific inclination angles can vary among individuals. The angle formed with the vertical axis typically ranges from 68° to 88°, while the angle with the sagittal plane falls within the range of 69° to 99° [23, 24]. These variations reflect the anatomical differences and individual characteristics of ankle joints. For a visual representation, please refer to Figure 3, which illustrates the orientation and inclinations of the tibiotalar joint axis in relation to the surrounding anatomical structures.

The rotation axis of the subtalar joint is also inclined, which is generally considered to be inclined upward at 42°, and inward at 23° with the vertical axis of the foot. There are great individual differences in the inclination of the rotation axis. The inclination angle of the subtalar joint is 21°–69° and the deflection angle is 4°–47° [24], as shown in Figure 4. The shaded areas are the range of the inclination and deflection angle of the subtalar joint respectively, and the blue line represents the average value.

In summary, the ankle joint is a composite joint composed of the tibiotalar joint and subtalar joint, and the axes of the two joints are not intersected, which is a

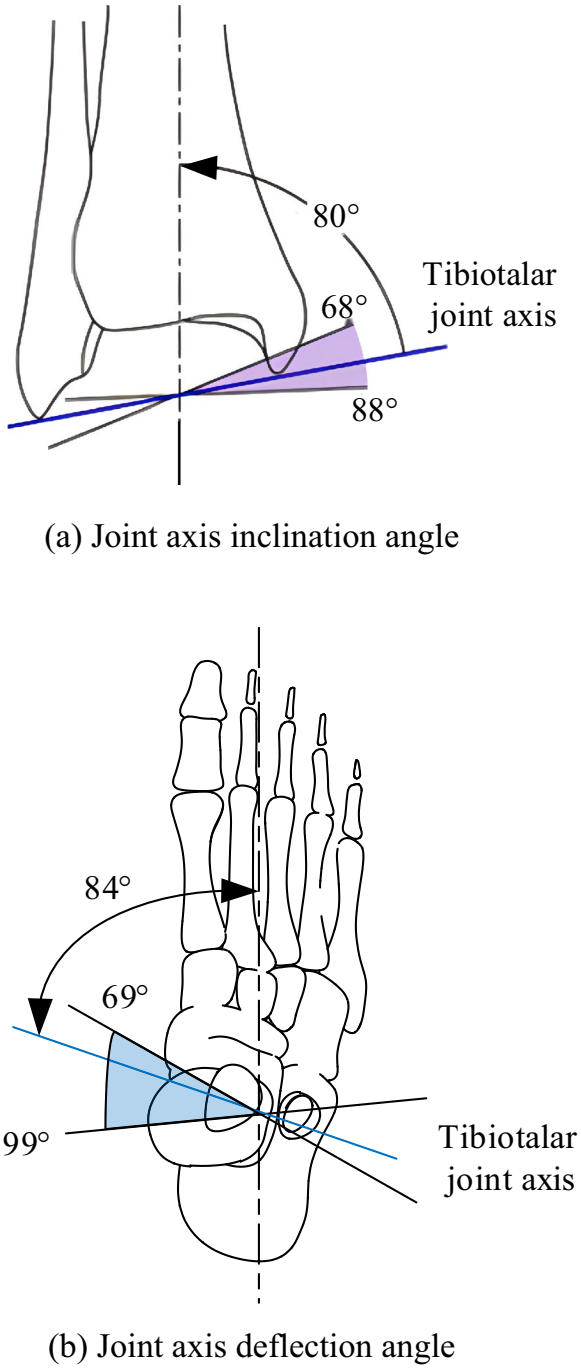

Figure 3 The rotation axis of the tibiotalar joint [25]

spatial interfacial relationship. If the rehabilitation robot does not match the actual anatomical model of the human ankle joint, it will make it difficult to ensure the rehabilitation effect and easy to cause secondary damage to the ankle joint. In addition, for different patients, the directions of the tibiotalar joint axis and subtalar joint axis are quite different, which means that most

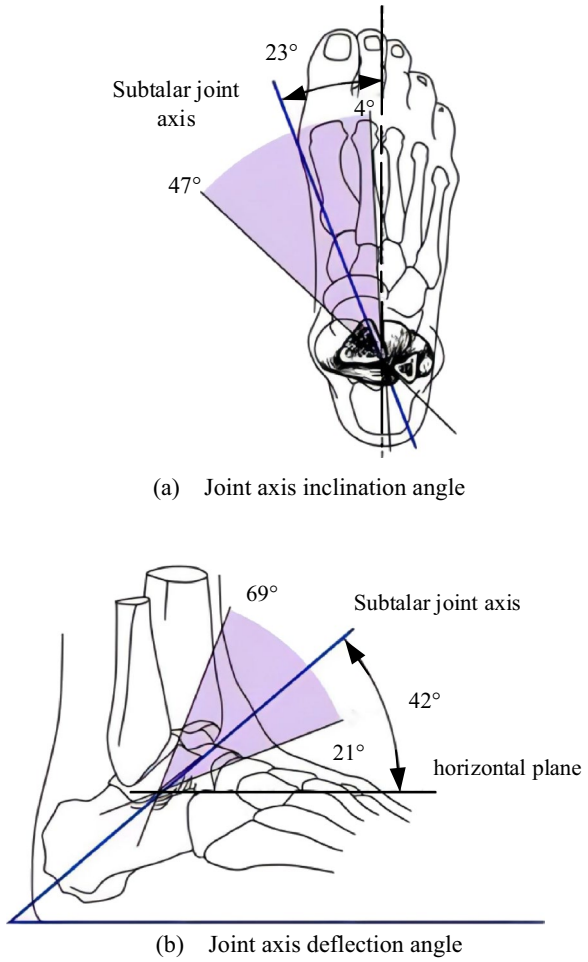

Figure 4 The rotation axis of the subtalar joint [26]

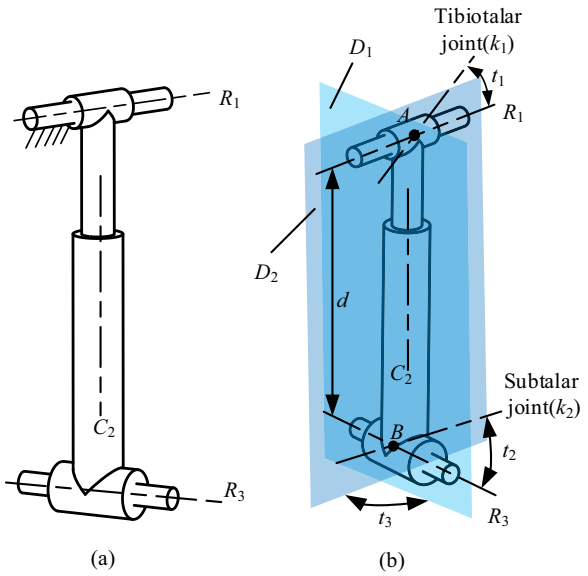

Figure 5 The mechanism diagram of the RCR model

rehabilitation robots are difficult to meet the rehabilitation needs of different individual patients.

Therefore, the physiological structure of the ankle joint is mainly related to the following four parameters: the inclination of the tibiotalar joint axis t_1, the inclination of the subtalar joint axis t_2, the deflection angle t_3 between the tibiotalar joint axis and the subtalar joint axis, and the distance d between the brain subtalar joint and the center point of the subtalar joint. Furthermore, the human ankle can be equivalent to a series RCR branch chain, as shown in Figure 5.

2.2 Establishment of Human Ankle Joint Equivalent Model

2.2.1 Mobility Analysis of the RCR Equivalent Model of Ankle Joint

The RCR mechanism has the following constraint relations: $R_1 \perp C_2$; $R_3 \perp C_2$; R_1 and C_2 intersect at point A, point A is fixed; R_3 and C_2 intersect at point B, and point B is stationary relative to the mobile platform. Establish the branch coordinate system as shown in Figure 6.

The establishment rules are as follows: the origin is defined on the fixed rotation center point A, the x-axis direction is parallel to the R_1 axis direction, the z-axis direction is along the translational direction of cylindrical joint C_2, and the y-axis direction is determined by the right-hand rule. The motion screw of each joint of the branch is:

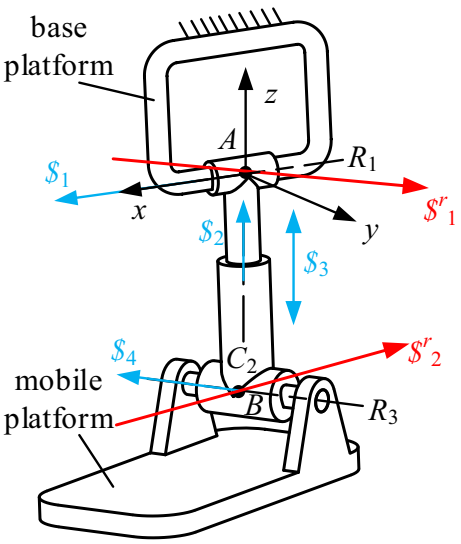

Figure 6 The mechanism diagram of the RCR equivalent model of ankle joint

$$\begin{cases} \$_1 = \left(1\ 0\ 0\ 0\ 0\ 0\right)^{\mathrm{T}}, \\ \$_2 = \left(0\ 0\ 1\ 0\ 0\ 0\right)^{\mathrm{T}}, \\ \$_3 = \left(0\ 0\ 0\ 0\ 0\ 1\right)^{\mathrm{T}}, \\ \$_4 = \left(a\ b\ 0\ c\ e\ 0\right)^{\mathrm{T}}. \end{cases} \tag{1}$$

Among them, a, b, c, e, and other parameters are related to the position and direction of the kinematic joint. It can be found that the constraint screw of this branch is

$$\begin{cases} \$_1^r = \left(a\ b\ 0\ 0\ 0\ 0\right)^{\mathrm{T}}, \\ \$_2^r = \left(1\ 0\ 0\ 0\ d\ 0\right)^{\mathrm{T}}, \end{cases} \tag{2}$$

It can be seen that the RCR branch has two constraint line vectors $\$_1^r$ and $\$_2^r$; $\$_1^r$ crossing point A and parallel to the R_3 direction of the revolute joint; $\$_2^r$ passes point B and is parallel to the direction of revolute joint R_1, as shown in Figure 6.

The two constraint forces limit the two translational DOFs of the RCR branch, and the mobile platform can translate along the direction of the connection line AB and rotate around the direction of the connection line AB. The mechanism can continuously rotate around any axis coplanar with the R_3 axis at point A, or around any axis coplanar with the R_1 axis at point B.

2.2.2 Configuration Design of the Parallel Rehabilitation Mechanism

According to the motion and constraint characteristics of the RCR model obtained above, the motion characteristics of the equivalent RCR parallel mechanism are given.

Motion characteristics 1: The mechanism has two virtual rotation centers, one virtual rotation center position is fixed, called fixed center A, and another virtual rotation center is called moving center B, point B remains relatively static with the mobile platform.

Motion characteristics 2: The mobile platform can move along the A and B connecting lines, and can rotate continuously around the A and B connecting lines.

Motion characteristics 3: The mobile platform has four DOFs for three rotations and one translation.

Corresponding to the motion characteristics, the constraint characteristics of the equivalent RCR parallel mechanism are as follows.

Constraint characteristics 1: The mobile platform is constrained by two constraint force screws, and two constraint force screws are not in one plane.

Constraint characteristics 2: The mobile platform is subjected to two constraint screws, one of them always passes through fixed point A, but the direction changes and the other always passes through moving point B, but the direction remains unchanged.

The design diagram of the equivalent RCR parallel mechanism is shown in Figure 7.

When the mechanism has m limbs, the constraint screw system of the mobile platform is the largest linear independent group of the union of the constraint screw systems of each limb. The constraint screw system of the mobile platform can be expressed as:

$$\$^r = \bigcup_1^m \$_j^r,\ j = 1, ..., m, \tag{3}$$

where $\$^r$ represents the constraint screw system of the moving platform; $\$_j^r$ represents the constraint screw system of the j-limb. The constraint screw system of the RCR model is known by Eq. (2), and the motion screw of the basic constraint screw system can be obtained. Taking point A as the origin, based on the reciprocal product principle, the basic motion screw of $\$_1^r$ is:

$$\begin{cases} \$_{m1} = \left(1\ 0\ 0\ 0\ 0\ 0\right)^{\mathrm{T}}, \\ \$_{m2} = \left(0\ 1\ 0\ 0\ 0\ 0\right)^{\mathrm{T}}, \\ \$_{m3} = \left(0\ 0\ 1\ 0\ 0\ 0\right)^{\mathrm{T}}, \\ \$_{m4} = \left(0\ 0\ 0\ 0\ 0\ 1\right)^{\mathrm{T}}, \\ \$_{m5} = \left(1\ 0\ 0\ 0\ 1\ 0\right)^{\mathrm{T}}. \end{cases} \tag{4}$$

The obtained basic motion screw system is linearly combined as follows:

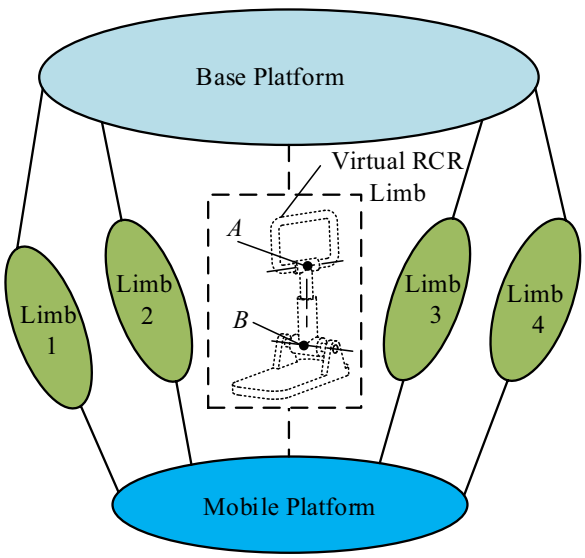

Figure 7 The design diagram of the equivalent RCR parallel mechanism

$$\begin{cases} \$_1 = \begin{pmatrix} 1 & 0 & 0 & 0 & 0 & 0 \end{pmatrix}^{\mathrm{T}}, \\ \$_2 = \begin{pmatrix} 0 & 1 & 0 & 0 & 0 & 0 \end{pmatrix}^{\mathrm{T}}, \\ \$_3 = \begin{pmatrix} 0 & 0 & 1 & 0 & 0 & 0 \end{pmatrix}^{\mathrm{T}}, \\ \$_4 = \begin{pmatrix} 0 & 0 & 0 & 0 & 0 & 1 \end{pmatrix}^{\mathrm{T}}, \\ \$_5 = \begin{pmatrix} 1 & 0 & 0 & 0 & a & 0 \end{pmatrix}^{\mathrm{T}}, \end{cases} \tag{5}$$

where $\$_1$, $\$_2$, and $\$_3$ can be equivalent to three revolute joints whose rotational axes intersect at a point, and these three revolute joints can be equivalent to a spherical joint. $\$_4$ is the prismatic joint, and $\$_5$ is a revolute joint whose axis is in the direction of the x-axis without passing the origin. At this point, the equivalent series branch of $\$_1^r$ can be obtained from Eq. (5), as shown in Figure 8(a). The branch is the SPR branch satisfying the constraint screw $\$_1^r$, but the rotation center of the SPR branch is the physical center A of the spherical joint rather than the virtual rotation center. Therefore, a further linear combination of Eq. (5) is needed, the motion screw system in Eq. (5) is linear combined again, and the following motion screw system is obtained:

$$\begin{cases} \$_1 = \begin{pmatrix} 0 & 0 & 1 & 0 & 0 & 0 \end{pmatrix}^{\mathrm{T}}, \\ \$_2 = \begin{pmatrix} 0 & m_1 & n_1 & 0 & 0 & 0 \end{pmatrix}^{\mathrm{T}}, \\ \$_3 = \begin{pmatrix} 1 & 0 & 0 & 0 & 0 & a \end{pmatrix}^{\mathrm{T}}, \\ \$_4 = \begin{pmatrix} 0 & 0 & 0 & 0 & m_2 & n_2 \end{pmatrix}^{\mathrm{T}}, \\ \$_5 = \begin{pmatrix} 1 & 0 & 0 & 0 & m_3 & n_3 \end{pmatrix}^{\mathrm{T}}. \end{cases} \tag{6}$$

Based on the concept of a virtual remote motion center, there should be at least two rotational screws in the motion screw system, and the two rotational screws need to intersect at point A of the virtual rotation center. Taking point A of the rotation center as the origin, $\$_1$ is the revolute joint of the axis along the z-axis and passing through the origin A; $\$_2$ is a revolute joint on the y-z plane and passes through the origin A, and $\$_1$ and $\$_2$ intersect at point A; $\$_3$ is a revolute joint of axes along the x-axis and not passing the origin A; $\$_4$ is the prismatic joint of the axis on the y-z plane; $\$_5$ is the revolute joint of the axis along the x-direction and does not pass through the origin, and $\$_3$ is parallel and does not coincide with $\$_5$. Therefore, the motion screw system in Eq. (6) can be equivalent to a RUPR branch, as shown in Figure 8(b). The branch can satisfy the constraint condition of the constraint screw $\$_1^r$ and has a virtual remote center point A, and point A is fixed. The constraint screw $\$_1^r$ always passes through point A. Similarly, the motion screw system satisfying the constraint screw $\$_2^r$ can be obtained, and then the constraint branch satisfying the $\$_2^r$ condition is obtained. The branch is the RPUR branch, which is opposite to the installation order of the RUPR branch and has a virtual motion center point B, point B is the moving point, but is fixedly connected to the mobile platform.

In summary, based on the motion screw system and constraint screw system of the RCR ankle joint equivalent model, two constraint branches of parallel rehabilitation mechanism are designed: RUPR branch and RPUR branch, which have a fixed virtual rotation center A and a follower virtual rotation center B, respectively. By adding two unconstrained UPS branches as the driving branches, a novel 4-DOF parallel ankle rehabilitation robot can be designed.

The novel ankle rehabilitation robot, as shown in Figure 9, is composed of a base platform, two circular slide rails, four electric push rods, and a mobile platform. It is controlled by the expansion and contraction of four electric cylinders to control the pitch, roll, deflection, and

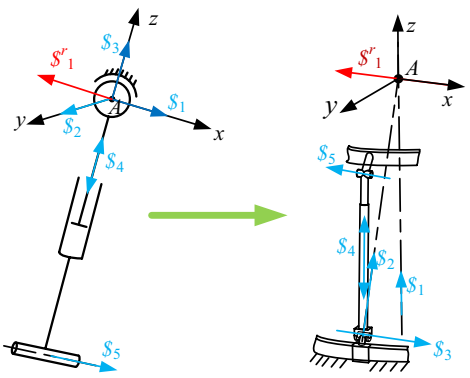

(a) The SPR branch chain (b) The RUPR branch chain

Figure 8 The design diagram of the constraint branch of the parallel mechanism

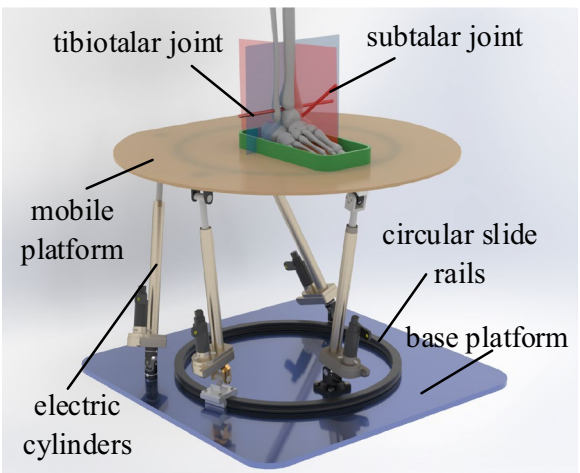

Figure 9 The CAD diagram of the rehabilitation robot

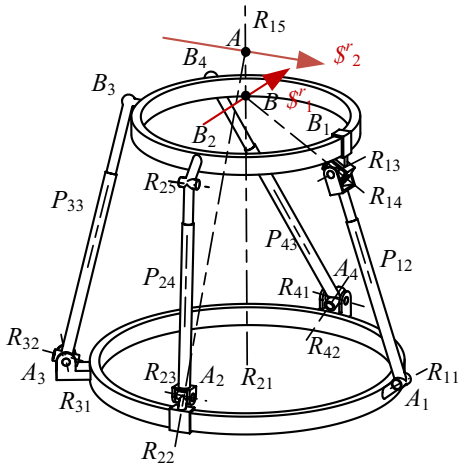

Figure 10 The structure of RPUR/RUPR/2-UPS PMs

lift of the mobile platform. The schematic diagram of the mechanism is shown in Figure 10.

As shown in Figure 10, the rehabilitation mechanism consists of a base platform $A_1A_2A_3A_4$, a mobile platform $B_1B_2B_3B_4$, two identical UPS branches, one RPUR branch, and one RUPR. The RPUR branch is connected to the mobile platform by a circular slide rail, which can be equivalent to a revolute joint. The rotation axis of the circular slide rail of the mobile platform is R_{15}, which is fixed to the mobile platform, and changes with the movement of the mobile platform. The RUPR branch is also connected with the base platform by a circular slide rail, which can also be equivalent to a revolute joint. The rotation axis of the sliding rail of the base platform is R_{21}, which is fixed and unchanged. Under the initial assembly configuration, the axis of R_{15} and the axis of R_{21} are coaxial.

Each universal joint is composed of two mutually perpendicular revolute joints such that R_{ij} represents the jth revolute joint in the ith branch of the mechanism, and P_{ij} is the prismatic joint in the ith branch of the mechanism. In Figure 10, the RPUR/RUPR/2-UPS mechanism has the following constraint relations: $R_{11} \perp P_{12}$; $R_{11} \| R_{13}$; $R_{23} \perp P_{24}$; $R_{23} \| R_{25}$; R_{21} and R_{22} intersect at A point, point A is fixed; R_{14} and R_{15} intersect at B point, point B is stationary relative to the mobile platform.

Since the UPS branch is a 6-DOF unconstrained branch, it is only necessary to analyze the RUPR branch and RPUR branch when analyzing the mobility of the ankle rehabilitation robot. It can be seen that the constraint line vector $\$_2^r$ passes through point A and is parallel to the axis direction of revolute joint R_{23}. The RUPR branch has the same structure as the RPUR, only the installation sequence is reversed, and the same analysis can be carried out. The constraint screw $\$_1^r$ of the RUPR branch passes through point B and is parallel to the axis of the revolute joint R_{11}. The constraint force of the two branches on the platform is staggered and passes through point A and point B respectively, as shown in Figure 10.

The two constraint line vectors limit the two translational DOFs of the mechanism. The mobile platform can move along the direction of the centerline AB and can realize three rotational degrees of freedom. Since the twist screw and wrench screw are instantaneous, they can only describe the motion and constraint of the mechanism in the instantaneous state, so it is necessary to verify the full-cycle mobility of the mechanism. For the rehabilitation mechanism, it is particularly important to have an axis that can realize continuous rotation. It can avoid a certain movement when the mechanism rotates, thus causing secondary damage to the human body. Therefore, it is necessary to distinguish the continuous rotation axis of the rehabilitation mechanism.

3 Discrimination of Full-cycle Mobility and Continuous Rotation Axis

3.1 The Full-cycle Mobility of the Mechanism

In the constraint branch, the two revolute joints adjacent to the prismatic joint are parallel to each other, and the three motion joints are always in the same plane, which can form a motion plane. For example, in the RUPR branch, the prismatic joint P_{12} and the revolute joints R_{11} and R_{13} form a plane M_1; In the RPUR branch, the prismatic joint P_{24} and the revolute joints R_{23} and R_{25} form a plane M_2; This means that the branch can move in a plane, and the inclination angle of the plane can be changed by two revolute joints of the axis in the plane. For example, in the RUPR branch, the plane M_1 can rotate around the sliding rail axis R_{15} of the mobile platform and the rotation axis R_{14}; In the RUPR branch, plane M_2 can rotate around the base platform slide rail axis R_{21} and rotation axis R_{22}. Plane M_1 intersects plane M_2 to form a straight line, as shown in Figure 11.

It can be seen from Figure 11 that axis R_{21} and axis R_{22} always intersect at fixed point A, so plane M_2 rotates around the fixed point A; the axis R_{14} and the axis R_{15} always intersect at the moving point B, so plane M_1 rotates around the moving point B. Therefore, the intersection of planes M_1 and M_2 is always the centreline of points A and B. Because the motion of the parallel mechanism mobile platform is the intersection of branch motions, based on the motion plane intersection theory [27], the mobile platform can move along the direction of the centreline of points A and B and rotate around the centreline of AB. In addition, because the connecting centerlines A and B incline at different angles along with different directions with the inclination of the motion

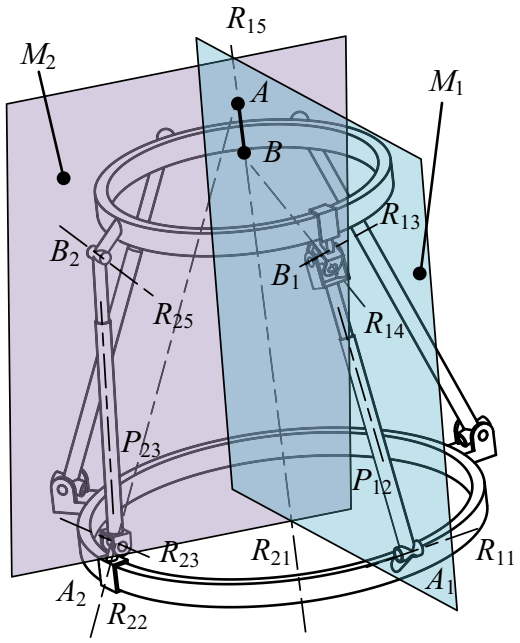

(a) Initial configuration of mechanism

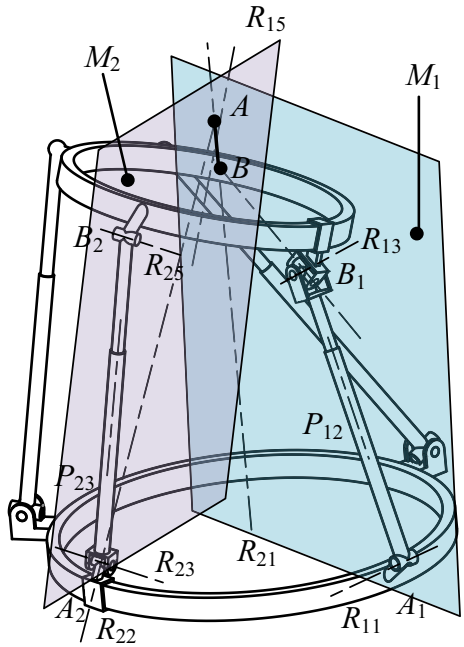

(b) General configuration of mechanism

Figure 11 Motion plane of mechanism constrained branch

plane, the mobile platform also has two other rotational degrees of freedom. To sum up, the mobile platform still has four degrees of freedom for three rotations and one translation under the general configuration.

3.2 Discrimination of Continuous Rotation Axis of the Mechanism

From the previous analysis, it can be seen that the mobile platform is subject to two constraint force line vectors: $\$_1^r = \left(f\boldsymbol{s}_1^r; \boldsymbol{r}_B \times f\boldsymbol{s}_1^r\right)$, $\$_2^r = \left(f\boldsymbol{s}_2^r; \boldsymbol{r}_A \times f\boldsymbol{s}_2^r\right)$, and the rotation of the mobile platform is defined as: $\$ = (\omega\boldsymbol{s}; \boldsymbol{r}_P \times \omega\boldsymbol{s})$. Based on the screw theory, the work of the constraint force line vector on the motion of the mobile platform is zero, that is, the constraint power is zero, and the following relationship should be satisfied:

$$\begin{cases} P_1^r = f\boldsymbol{S}_1^r \circ \omega\$ = f\omega\boldsymbol{r}_{BP} \cdot \left(\boldsymbol{s}_1^r \times \boldsymbol{s}\right) = 0, \\ P_2^r = f\boldsymbol{S}_2^r \circ \omega\$ = f\omega\boldsymbol{r}_{AP} \cdot \left(\boldsymbol{s}_2^r \times \boldsymbol{s}\right) = 0. \end{cases} \tag{7}$$

From the above equation, it can be concluded that the pure rotation axis allowed by the mobile platform needs to be parallel or intersected at the constraint force line vector. However, the rotation axis satisfying these conditions, including the continuous rotation axis and the instantaneous rotation axis, is further judged by the constraint power and its derivative in this paper. That is, when the constraint power is zero [28], the rate of change of the constraint power also needs to be zero.

$$\begin{cases} \dot{P}_1^r = \frac{\mathrm{d}}{\mathrm{d}t}\left(f\omega\boldsymbol{r}_{BP} \cdot \left(\boldsymbol{s}_1^r \times \boldsymbol{s}\right)\right) = 0, \\ \dot{P}_2^r = \frac{\mathrm{d}}{\mathrm{d}t}\left(f\omega\boldsymbol{r}_{AP} \cdot \left(\boldsymbol{s}_2^r \times \boldsymbol{s}\right)\right) = 0. \end{cases} \tag{8}$$

When the rotating axis is a continuous rotating axis, it has the following constraints: $\boldsymbol{r}_{BP} \cdot \left(\boldsymbol{s}_1^r \times \boldsymbol{s}\right) = 0$, $\boldsymbol{r}_{AP} \cdot \left(\boldsymbol{s}_2^r \times \boldsymbol{s}\right) = 0$, the direction of the rotating axis is constant ($\dot{\boldsymbol{s}} = 0$), the direction of the constraint force is determined ($\dot{\boldsymbol{s}}_i^r = 0$), and the constraints are brought into Eq. (8). Therefore, the necessary and sufficient conditions for the existence of the continuous rotating axis of the mobile platform are as follows:

$$\begin{cases} \boldsymbol{r}_{BP} \cdot \left(\boldsymbol{s}_1^r \times \boldsymbol{s}\right) = 0, \\ \boldsymbol{r}_{AP} \cdot \left(\boldsymbol{s}_2^r \times \boldsymbol{s}\right) = 0, \\ \left(\boldsymbol{s} \times \boldsymbol{r}_{BP}\right) \cdot \left(\boldsymbol{s}_1^r \times \boldsymbol{s}\right) = 0, \\ \left(\boldsymbol{s} \times \boldsymbol{r}_{AP}\right) \cdot \left(\boldsymbol{s}_2^r \times \boldsymbol{s}\right) = 0. \end{cases} \tag{9}$$

If $\boldsymbol{s}$ is parallel to $\boldsymbol{s}_1^r$ and $\boldsymbol{s}_2^r$ respectively, that is, $\left(\boldsymbol{s}_1^r \times \boldsymbol{s}\right) = 0$, $\left(\boldsymbol{s}_2^r \times \boldsymbol{s}\right) = 0$, then the Eq. (5) is satisfied.

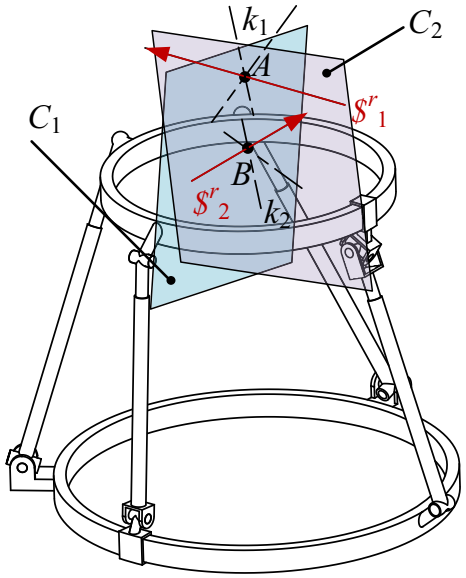

Figure 12 Schematic diagram of the continuous rotation axis of the mechanism

Otherwise, $\boldsymbol{s}$ is required to intersect with $\boldsymbol{s}_1^r$ and $\boldsymbol{s}_2^r$ respectively, and $(\boldsymbol{s} \times \boldsymbol{r}_{BP}) = 0$, $(\boldsymbol{s} \times \boldsymbol{r}_{AP}) = 0$, that is, the rotation axis passes the constraint point A or B. Therefore, the continuous rotation axis of the mechanism is shown in Figure 12.

It can be seen from Figure 12 that the mobile platform can realize continuous rotation around any axis k_1 that is coplanar (parallel or intersecting) with the constraint force line vector and bypasses the constraint force point A. The axis k_1 forms a rotational plane C_1, and any axis passing point A on the plane C_1 is a continuous rotation axis. Similarly, the mobile platform can rotate continuously around any axis k_2 that is coplanar (parallel or intersecting) with the constraint force line vector and bypass constraint force point B, and the axis k_2 forms a rotating plane C_2. Any straight line crossing point B on plane C_2 is a continuous axis. The intersection line of plane C_1 and plane C_2 is always the center line of point A and point B.

In rotation plane C_1, there is a tilt axis k_1 over the fixed point A, which can match the human tibiotalar joint axis. In rotation plane C_2, there is a tilt axis k_2 over the moving point B, which can match the human subtalar joint axis. The rotation axis k_1 is the fixed axis, which is stationary. The rotation axis k_2 is the moving axis, which rotates with the rotation of k_1, but remains unchanged relative to the mobile platform and human plantar. The length of the connection line AB can be adjusted by translational DOF to adapt to the difference in ankle height of different patients. By selecting the appropriate tilt axis in the C_1, and C_2 planes to adapt to the different individual joint axis inclinations; the angle between plane C_1 and plane C_2 can be adjusted by the rotational DOF around the connection line AB to adapt to the difference in the deflection angle between the joint axes of different individuals.

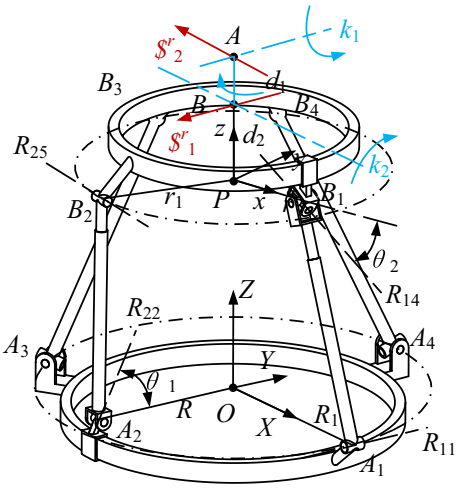

Figure 13 The RPUR/RUPR/2UPS mechanism parameters

4 Inverse Kinematics Analysis

The coordinate system is established as shown in Figure 13. The origin O of the global coordinate system O-XYZ is the center of the fixed platform $A_1A_3A_4$. The Y-axis is along the axis direction of the revolute joint R_{11}, and the Z-axis is along the normal direction of the base platform. Similarly, the mobile coordinate system P-xyz is established, and P is the center of the mobile platform $B_2B_3B_4$. The following parameters are defined: the circumcircle radius of triangle $A_1A_3A_4$ is R_1, the circumcircle radius of triangle $B_2B_3B_4$ is r_1, the length of platform slide radius OA_2 is R, the length of mobile platform slide radius PB_1 is r, the length of connection center line AB is d_1, and the length of connection line BP is d_2. The inclination angle of the axis of the revolute joint R_{22} is θ_1, and the inclination angle of the axis of the revolute joint R_{14} is θ_2.

Then in the global coordinate system O-XYZ, the coordinates of points A and B can be expressed as:

$$\begin{cases} \boldsymbol{A} = [0, 0, R \cdot \tan(\theta_1)]^{\mathrm{T}}, \\ \boldsymbol{B} = {}^{O}\boldsymbol{R}_P \cdot {}^{P}\boldsymbol{B} + \boldsymbol{P}, \end{cases} \tag{10}$$

where ${}^{O}\boldsymbol{R}_P$ is the attitude matrix of the mobile platform, $\boldsymbol{B}^P = [0, 0, r \cdot \tan(\theta_2)]^{\mathrm{T}}$, $\boldsymbol{P} = [x, y, z]^{\mathrm{T}}$.

The attitude of the mobile platform can be determined by the length d_1 of the connecting line AB, the continuous rotation σ_1 around the k_1 axis, the continuous rotation σ_2 around the connecting line AB, and the continuous rotation σ_3 around the k_2 axis. The k_1 axis is an

axis passing point A on the continuous rotation plane C_1 and is parallel to the constraint force line vector $\$_2^r$ along the direction of the Y-axis. The k_2 axis is an axis passing point B on the continuous rotation plane C_2 and is parallel to the constraint force line vector $\$_2^r$. Under the initial assembly configuration, the angle between planes C_1 and C_2 is $\pi/2-\sigma_0$, because the human body generally tilts 23° inward from the subtalar joint, so σ_0 can be set to 23°.

In summary, the motion of the mobile platform can be equivalent to a 4-DOF RPRR series manipulator, rotating around the k_1 axis, moving around the connection line AB, rotating around the connection line AB, and rotating around the k_2 axis. Therefore, the homogeneous transformation matrix is as follows:

$$\begin{aligned} {}^{A}\boldsymbol{T}_P &= \boldsymbol{T}_y(\sigma_1)\boldsymbol{T}_z(\sigma_0+\sigma_2)\boldsymbol{t}_z(-d_1)\boldsymbol{T}_x(\sigma_3)\boldsymbol{t}_z(-d_2)\boldsymbol{T}_z(-\sigma_0) \\ &= \begin{bmatrix} r_{11} & r_{12} & r_{13} & x_a \\ r_{21} & r_{22} & r_{23} & y_a \\ r_{31} & r_{32} & r_{33} & z_a \\ 0 & 0 & 0 & 1 \end{bmatrix} = \begin{bmatrix} {}^{O}\boldsymbol{R}_P & {}^{A}\boldsymbol{P} \\ 0 & 1 \end{bmatrix}. \end{aligned} \tag{11}$$

The position coordinates of point P and the attitude matrix ${}^{O}\boldsymbol{R}_P$ of the mobile platform can be obtained by Eq. (11), $\boldsymbol{P}=\boldsymbol{A}+{}^{A}\boldsymbol{P}$. Since points B_2, B_3 and B_4 are respectively fixed on the mobile platform, the coordinates of points B_2, B_3, and B_4 can be obtained from the following:

$$\boldsymbol{B}_i = {}^{O}\boldsymbol{R}_P \cdot {}^{P}\boldsymbol{B}_i + \boldsymbol{P}, (i=2,3,4). \tag{12}$$

Since point B_1 is always in the XZ plane and slides relative to the mobile platform, the coordinates of point B_1 can be defined as $[B_{1x},0,B_{1z}]$. Since the distance from point B_1 to point P and point B is always constant, there are the following constraints:

$$\begin{cases} |\boldsymbol{P}-\boldsymbol{B}_1| = r, \\ |\boldsymbol{B}-\boldsymbol{B}_1| = \sqrt{r^2+d_2^2}. \end{cases} \tag{13}$$

Similarly, since the A_2 point is always in the XY plane and sliding relative to the base platform, the coordinates of point A_2 can be defined as $[A_{2x},A_{2y},0]$. Because the distance between point A_2 and point O is constant, and the line A_2B_2 is always perpendicular to the axis of R_{25}, $\boldsymbol{s}_{25}$ is defined as the direction vector of R_{25}, there are the following constraints:

$$\begin{cases} |\boldsymbol{O}-\boldsymbol{A}_2| = R, \\ \boldsymbol{AB}\cdot({}^{O}\boldsymbol{R}_P\cdot\boldsymbol{s}_{25}) = 0. \end{cases} \tag{14}$$

Through Eqs. (13) and (14), the coordinates of points B_1 and A_2 in the global coordinate system can be solved respectively. Finally, the length of each branch prismatic joint is obtained:

$$L_i = |\boldsymbol{B}_i - \boldsymbol{A}_i|. \tag{15}$$

5 Kinematic Performance and Workspace Analysis of the Mechanism

5.1 Wrench the Screw and Twist the Screw of the Mechanism

When the input twist screw (ITS) in the branch is locked, there will be one more constraint screw $\$_{Ti}$, $\$_{Ti}$ is the transmission wrench screw (TWS) of the branch, and the reciprocal product of the transmission wrench screw and other twist screws is zero. $\$_i^r$ is the branch constraint wrench screw; $\$_{Oi}$ is the output twist screw of the mobile platform; $\$_{Ri}$ is the branch limited twist screw, and $\triangle\ \$_{Oi}$ is the platform limited twist screw. There are the following relationships between them.

$$\begin{cases} \$_{Ti}\circ\$_{Oj}=0, & (i=1,2,3,4;\ i\neq j), \\ \$_j^r\circ\$_{Oi}=0, & (i=1,2,3,4;\ j=1,2), \\ \$_j^r\circ\triangle\ \$_{Oi}=0, & (j=1,2;\ j\neq i), \\ \$_{Ti}\circ\triangle\ \$_{Oj}=0, & (i=1,2,3,4;\ j=1,2). \end{cases} \tag{16}$$

The mechanism motion/force transmission indices can be subdivided into two parts: the input transmission index [8] (ITI) and the output transmission index [29] (OTI). Mechanism motion/force constraint indices can also be divided into two parts: input constraint index (ICI) and output constraint index [30, 31] (OCI).

$$\begin{cases} \lambda_{Ii} = \dfrac{|\$_{Ti}\circ\$_{Ii}|}{\max(|\$_{Ti}\circ\$_{Ii}|)}, \\ \lambda_{Oi} = \dfrac{|\$_{Ti}\circ\$_{Oi}|}{\max(|\$_{Ti}\circ\$_{Oi}|)}, \\ k_{Ii} = \dfrac{|\$_i^r\circ\$_{Ri}|}{\max(|\$_i^r\circ\$_{Ri}|)}, \\ k_{Oi} = \dfrac{|\$_i^r\circ\triangle\$_{Oi}|}{\max(|\$_i^r\circ\triangle\$_{Oi}|)}. \end{cases} \tag{17}$$

In Eq. (17), λ_{Ii} is the input transmission index of the ith branch; λ_{Oi} is the output transmission index of the ith branch; k_{Ii} is the input constraint index of the ith branch; k_{Oi} is the output constraint index of the ith branch, $\$_{Ii}$ is the input twist screw.

5.2 Transmission Performance Analysis

The transmission index is the power coefficient between the branch transmission wrench screw $\$_{Ti}$ and the branch input twist screw $\$_{Ii}$ and the platform output twist screw $\$_{Oi}$, and the input and output transmission indexes can be obtained from Eq. (17). Define the local transmission index (LTI) as follows:

$$\lambda = \min(\lambda_{Ii}, \lambda_{oi}). \tag{18}$$

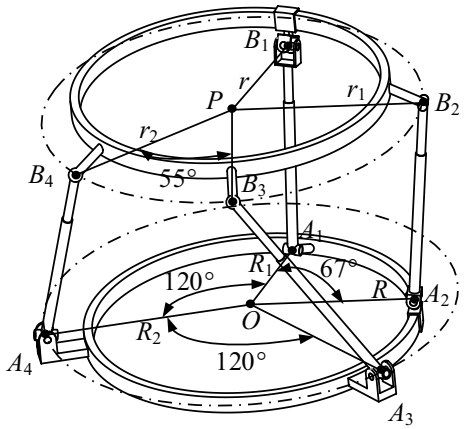

Figure 14 Parameters of rehabilitation mechanism

To describe the correlation between the configuration variables and the transmission performance of the mechanism, the exact size parameters of the mechanism are given for example analysis. As shown in Figure 14, $R = 180$ mm for the radius of the base platform slide rail, R_1 is the length of OA_1, R_2 is the length of OA_4, $R_1 = 120$ mm, $R_2 = 220$ mm; the sliding radius of the mobile platform is $r = 180$ mm, r_1 is the length of PB_2, r_2 is the length of PB_4, $r_1 = 220$ mm, $r_2 = 220$ mm, the angle between PB_3 and PB_4 is 55°, and the angle between OA_3 and OA_4 is 120°.

The distance between the axis of the tibiotalar joint and the axis of the subtalar joint is about 30 mm [32], so let $d_1 = 30$ mm, and λ_1 is the rotation angle around the axis of the tibiotalar joint of the human body, λ_2 is the rotation angle around the axis k_2 of the subtalar joint, and the axis of the tibiotalar joint is taken as the horizontal axis k_1, so $\lambda_1 = \sigma_1$; Because the subtalar joint is tilted inward by σ_0 degrees and upward by σ_{01} degrees (usually $\sigma_0 = 23$, $\sigma_{01} = 42$), there are:

$$\sigma_2 = \lambda_2 \cdot \sin(\sigma_{01}), \sigma_3 = \cos(\sigma_{01}). \tag{19}$$

The LTI atlas of the mechanism is drawn with λ_1 and λ_1 as coordinates, as exhibited in Figure 15.

It can be seen from Figure 15 that the transmission performance of the mechanism is good, and the transmission performance indexes of the mechanism in most regions are above 0.5. When the LTI value is less than 0.1, it can be considered that the transmission singularity occurs. The minimum LTI value in Figure 15 is 0.35, indicating that the mechanism is far from the singular configuration. When λ_1 is greater than 0, the transmission performance is better, that is, the performance of the right part of the LTI atlas is better than that of the left part; when λ_2 is less than 0, the transmission performance is better, that is, the lower part of the atlas has better transmission performance than the upper part; the greater the λ_2 angle, the worse the transmission performance of the mechanism.

5.3 Constraint Performance Analysis

The input constraint performance index k_{Ii} is the power coefficient between the branch constraint wrench screw $\$_i^r$ and the branch limited twist screw $\$_{Ri}$, and the output constraint performance index k_{Oi} is the power coefficient between the branch constraint force $\$_i^r$ and the mobile platform limited twist screw $\triangle\ \$_{Oi}$. Similarly, the local constraint index (LCI) is defined as follows:

$$k = \min(k_{Ii}, k_{oi}). \tag{20}$$

Similarly, the LCI atlas of the mechanism is drawn with the angle λ_1 of the human body around the tibiotalar

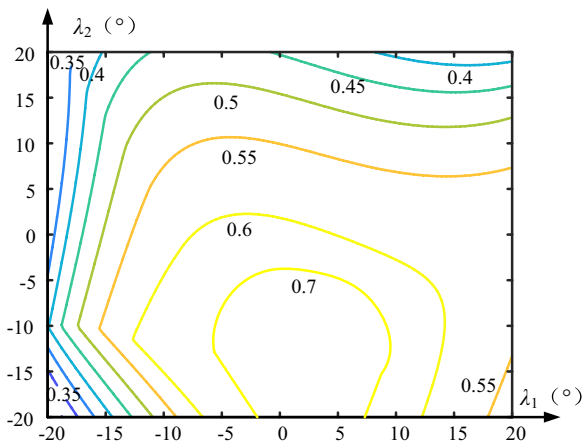

Figure 15 Contour of LTI

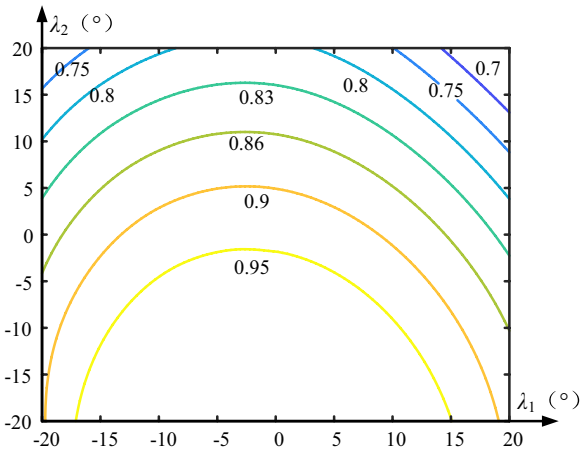

Figure 16 Contour of LCI

joint and the angle λ_2 of the subtalar joint as coordinates, as shown in Figure 16.

It can be seen from Figure 16 that the mechanism constraint performance is excellent. The mechanism constraint performance index is basically above 0.8, and the minimum value is 0.7, which is far from the singular configuration. There is no constraint singularity in the atlas. The left and right sides of the constraint atlas are basically the same, and the axis of $\lambda_1 = 0$ is approximately symmetrical. The smaller λ_2 is, the better the constraint performance of the mechanism is, and the larger the value of λ_2 is, the worse the constraint performance of the mechanism is. When λ_1 is equal to 0, the constraint performance of the mechanism is the best. With the increase of the absolute value of λ_1, the constraint performance index of the mechanism decreases.

5.4 Workspace Analysis

Although the rehabilitation institution has four degrees of freedom of three rotations and one translation, it only performs rotational rehabilitation after matching the patient's physiological structure, so its rotational ability is mainly analyzed. In order to visually describe the motion attitude of the mechanism, a modified Euler angle proposed by Bonev et al. [33], namely the Tilt -and - Torsion (T&T) Euler angle, is used here. Compared with the traditional Euler angle, this T&T T Euler angle is more intuitive to describe the three-dimensional rotation of the mechanism, as shown in Figure 17. The inclination angle β is the angle between the z-axis of the mobile platform and the Z-axis of the global coordinate system, and the azimuth angle α is the angle between the projection of the z-axis of the mobile platform on the fixed XY plane and the fixed X-axis. γ represents the size of the torsion angle.

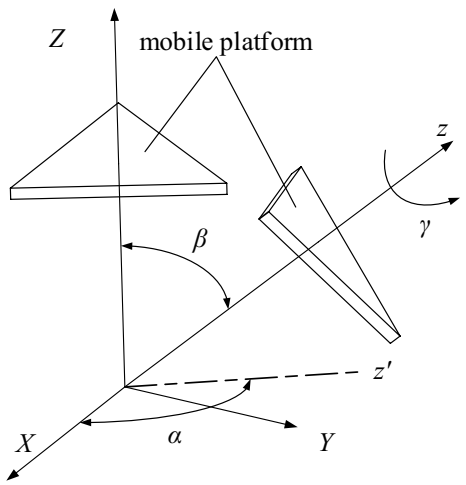

Figure 17 The T&T Euler angle

The attitude of the mobile platform is represented by the T&T Euler angle, and the attitude matrix of the mechanism is as follows:

$$
\begin{aligned}
{}^{O}\boldsymbol{R}_P &= \boldsymbol{R}_z(\alpha)\boldsymbol{R}_y(\beta)\boldsymbol{R}_z(-\alpha)\boldsymbol{R}_z(\gamma) \\
&= \begin{bmatrix} k_x^2\mathrm{Vers}\beta + c\beta & k_y k_x \mathrm{Vers}\beta & k_y s\beta \\ k_x k_y \mathrm{Vers}\beta & k_y^2\mathrm{Vers}\beta + c\beta & -k_x s\beta \\ -k_y s\beta & k_x s\beta & c\beta \end{bmatrix},
\end{aligned} \tag{21}
$$

where $s\beta = \sin\beta$, $c\beta = \cos\beta$, and $k_x = \cos(\alpha + \pi/2)$, $k_y = \sin(\alpha + \pi/2)$, $\mathrm{Vers}\beta = (1 - \cos\beta)$. Combined with Eq. (11), two attitude representation methods can be converted to each other.

The workspace of the ankle rehabilitation mechanism is mainly limited by the following factors: ① the range of motion of the driving joint; ② whether the mechanism is close to a singular configuration; ③ interference between branches; ④ maximum deflection angle of spherical joint.

$$
\begin{cases}
l_{\min} \le l_i \le l_{\max}, \\
\min(\lambda, k) \ge 0.1, \\
D \le D_{ij}, \\
q \le q_{\max}.
\end{cases} \tag{22}
$$

In Eq. (22), $l_{\min}$, $l_{\max}$ are the minimum and maximum values of the driving joint stroke; min (λ, k) is the minimum value of the transmission performance λ and constraint performance k of the mechanism. When min (λ, k) > 0.1, it shows that the mechanism does not have a singularity. D is the diameter of the branch electric push rod; D_{ij} is the distance between two branches; $q_{\max}$ is the maximum deflection angle of the spherical joint.

The boundary search method is used to solve the workspace, that is, by substituting all possible values of the attitude parameters into the inverse kinematics solution to see whether they meet the constraints of the mechanism, to determine whether the attitude is the point inside the workspace of the mechanism, so as to find all the points constituting the workspace of the mechanism. The dimension parameters of the mechanism are consistent with those above. When $l_{1\max} = l_{4\max} = 330$ mm, $l_{1\min} = l_{4\min} = 200$ mm, $l_{2\max} = l_{3\max} = 360$ mm, $l_{2\min} = l_{3\min} = 230$ mm, and $D = 30$ mm, $q_{\max} = 20°$, the rotation space of the rehabilitation mechanism can be searched. Here, the cylindrical coordinate system [34] is used to describe the rotation space of the mechanism, as shown in Figure 18. Three Euler angles (α, β, γ) are the angular coordinates, radial coordinates, and vertical coordinates of the cylindrical coordinate system.

It can be seen from Figure 18 that when the torsion angle is zero ($\gamma = 0°$), the rotation ability of the mechanism is the best, and the maximum inclination angle of the mechanism can be reached at 30°. When the

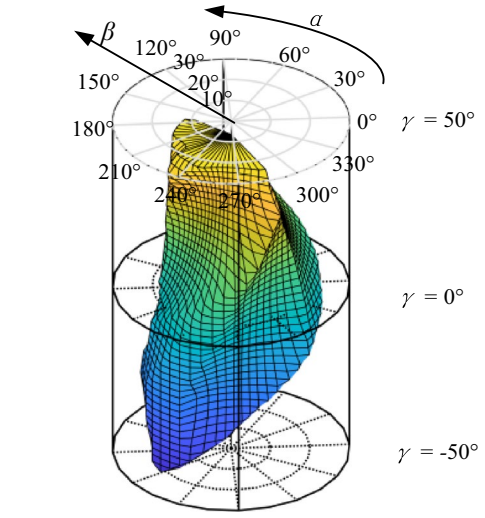

(a) Lateral view of rotational space

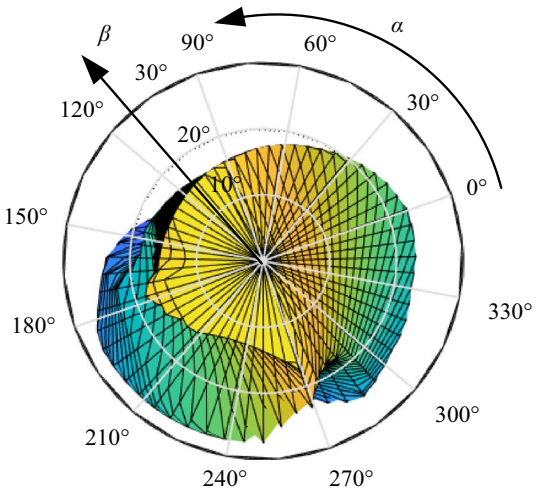

(b) Top view of rotational space

Figure 18 Mechanism rotational workspace

mechanism does not tilt ($\beta = 0°$), the maximum rotation range of the mechanism can reach (− 48°, 48°). In the range of azimuth angle α from 30° to 150°, the rotation ability is poor, and in the range of 160° to 250°, the rotation ability of the mechanism is the best. When $\gamma = 0°$, the minimum inclination angle of the mechanism is 18°, and at this time, the azimuth angle α is 110°.

6 Human-Machine Coupling Rehabilitation Simulation

A rehabilitation robot serves as a crucial tool in assisting patients with safe and comfortable rehabilitation therapy. Therefore, it is essential to evaluate the effectiveness

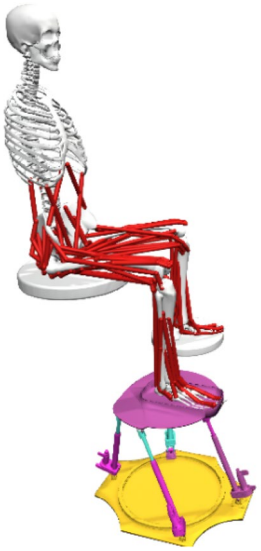

Figure 19 Human-machine coupling simulation model

of rehabilitation robots. Due to the complexities of the human bone structure and joints, as well as limitations in measuring instruments, the use of biomechanical analysis software has become a prominent trend for evaluating the effects of rehabilitation robots in the rehabilitation process. One widely utilized software in this domain is OpenSim [35]. OpenSim enables the simulation of musculoskeletal dynamics and neuromuscular control, providing an accurate biomechanical model for muscle dynamics and joint kinematics modeling. It accurately reproduces human and animal movements, making it applicable in various fields, including biomechanics research, surgical process simulation, and medical rehabilitation device development.

Rehabilitation therapy modes can be broadly categorized into three categories: passive rehabilitation, collaborative rehabilitation, and active rehabilitation [36]. The choice of rehabilitation mode depends on the extent of the patient's injury. In the early stage of rehabilitation, when the injured limbs may not respond, the passive rehabilitation mode is adopted [37]. During the middle stage of rehabilitation, the patient and the rehabilitation robot move together [38]. In the later stage of rehabilitation, when the patient has gained a certain level of muscle strength, impedance active rehabilitation therapy with a certain intensity can be conducted [36]. In this paper, we evaluate and analyze the effect of an ankle rehabilitation robot on passive rehabilitation of the human foot using OpenSim biomechanical software. The ankle rehabilitation robot model, established in SolidWorks software, is imported into OpenSim software. By setting the physiological parameters of the human body through OpenSim

XML language, we combine the human neuromuscular skeleton model with the rehabilitation robot to create a human-machine coupling model for rehabilitation simulation, as shown in Figure 19.

When wearing a rehabilitation robot on the human body, flexible materials such as elastic straps are usually used. On the one hand, they can constrain the movement of the human body and exert the functions of the rehabilitation robot, and on the other hand, they can protect the human body to a certain extent from harm, because the rehabilitation robot and the human body are actually not perfectly compatible. The rehabilitation mechanism's mobile platform is connected to the human foot through a BushingForce element. BushingForce is a 6-DOF spring damping force with three translations and three rotations, which can be free or constrained by flexible forces. It can establish moving springs/damping or rotating springs/damping in six directions, which can effectively simulate the flexible binding effect between human feet and the platform.

Based on the human-machine coupling model, the passive rehabilitation simulation is carried out for the early rehabilitation stage of patients with serious ankle injuries. At this time, the robot performs active motion according to the rehabilitation needs, drives the ankle joint to perform dorsiflexion/plantar flexion, inversion/eversion, and other actions, and the human ankle muscle follows the rehabilitation robot to passively stretch. The given motion of the tibiotalar joint and the subtalar joint is as follows:

$$\begin{cases} \lambda_1 = \frac{\pi}{12} \cdot \sin(0.5\pi t), \\ \lambda_2 = \frac{\pi}{15} \cdot \sin(0.4\pi t). \end{cases} \tag{23}$$

Foot movement is mainly controlled by the muscles on the lower leg. During the dorsiflexion / plantar flexion, and inversion/eversion movement of the foot, the muscles that play a major role include extensor digitorum longus, flexor digitorum longus, tibialis anterior, tibialis posterior, extensor hallucis longus, flexor hallucis longus, peroneus brevis, gastrocnemius, soleus, and so on. Therefore, the above muscles are selected as the analysis objects. Muscle activation, muscle passive force, muscle fiber length, and human-machine interaction force were selected as output parameters to evaluate the rehabilitation effect of the rehabilitation robot. During the rehabilitation process, the muscle force of the patient should not increase sharply to avoid foot discomfort, and the human-machine binding force curve and muscle fiber length curve should not produce violent fluctuations. When performing rehabilitation therapy according to the rehabilitation trajectory given by Eq. (23), the human-machine interaction force is the flexible binding force curve between the human foot and the rehabilitation robot, as shown in Figure 20; the activation of each muscle is shown in Figure 21; the length of each muscle fiber is shown in Figure 22; the passive tension of each muscle is shown in Figure 23.

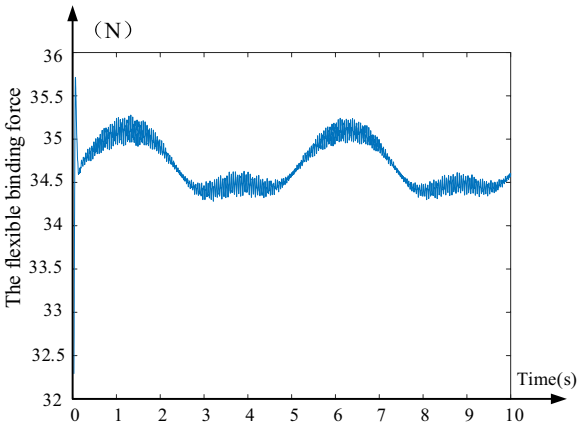

Figure 20 The flexible binding force curve

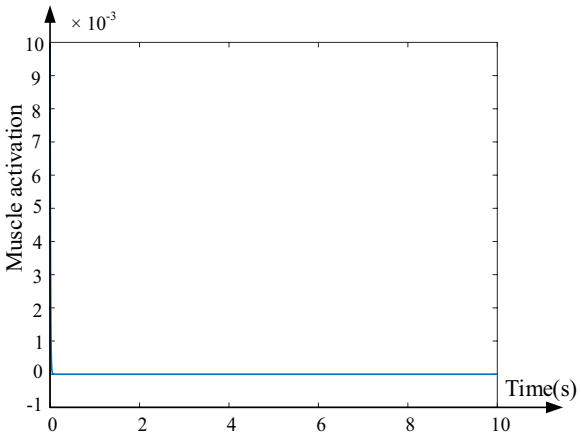

Figure 21 Ankle muscle activation curve

It can be seen from Figure 20 that the maximum human-machine flexible binding force is about 36 N, and the fluctuation range is small, which will not make the foot feel uncomfortable or hurt. Figure 21 shows that the muscle activation degree is 0, which means that the muscle is only passive stretching, and does not produce active force, in line with the patient's initial passive rehabilitation; it can be seen from Figure 22 that under the rehabilitation trajectory shown in Eq. (23), the transition of the muscle fiber length curve of the ankle joint is smooth, without sharp elongation, and will not cause discomfort to the patients. Under this rehabilitation trajectory, the variation trends of muscle length curves in Figure 22(a) are consistent, and they are synergistic muscles. Similarly, the muscles in Figure 22(b) are also synergistic muscles. The variation trends of muscle length curves in Figure 22

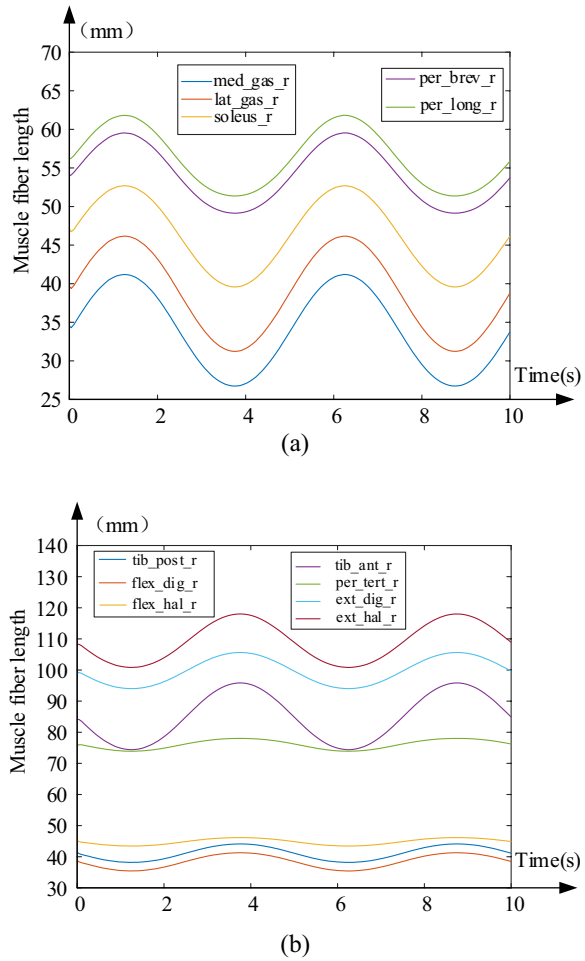

Figure 22 Ankle joint muscle fiber length curve

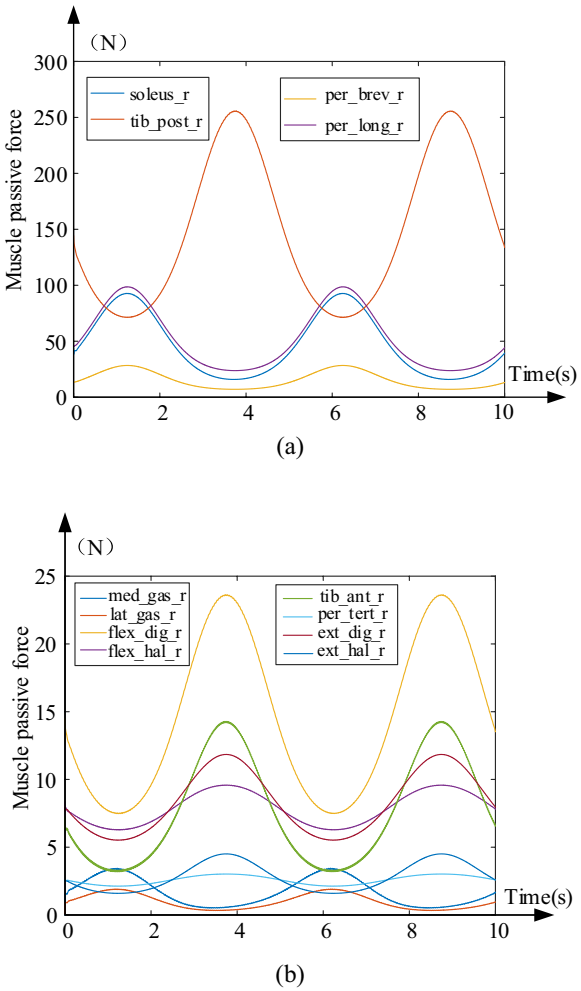

Figure 23 Ankle joint muscle passive force curve

are opposite, and they are antagonistic muscles. It can be seen from Figure 23 that the four muscles, i.e., tibialis posterior (tib_ post _ r), peroneus longus (per _ long _ r), soleus (soleus_ r), and peroneus brevis (per _ brev _ r), are subjected to the maximum force, while the other muscles are subjected to small tension. Among them, the maximum tension of the muscle is not more than 300 N, and the muscle curve is excessively smooth without rapid growth. In the rehabilitation process, it will not cause secondary damage to the ankle joint and will not make the human body uncomfortable.

7 Conclusions

In this study, we determined the equivalent model of an ankle rehabilitation robot based on the anatomical structure and motion properties of the human ankle. We established a mapping relationship between the human ankle and the configuration design of the rehabilitation mechanism.

(1) A novel 4-DOF ankle rehabilitation mechanism with three rotations and one translation was designed. This mechanism incorporates two virtual center points and offers several advantages, including human-machine motion matching, adaptability to different patients, convenient wearing, left and right foot switching, and high safety.

(2) The motion properties and full-cycle mobility of the mechanism were verified using the intersection theory of the motion plane. Two rotation planes were determined based on the constraint power and its derivative. On these rotation planes, the mechanism can achieve continuous rotation by bypassing any line of the virtual center point.

(3) The kinematic performance of the mechanism was analyzed based on the motion/force transmission index and constraint index. It was demonstrated that the rehabilitation mechanism exhibits good transmission performance and constraint perfor-

mance. The workspace of the mechanism was also analyzed, taking into account constraints such as singular configuration, driving stroke, and branch interference.

(4) A human-machine coupling rehabilitation simulation model was established using the OpenSim biomechanical software. The rehabilitation effect was evaluated using the change curves of human-machine flexible connection force, muscle fiber length, and muscle passive tension as evaluation indexes. This evaluation has significant implications for formulating rehabilitation strategies under the passive rehabilitation mode and serves as the foundation for subsequent prototype manufacturing and kinematic control.

8 Discussion

Although the proposed rehabilitation mechanism can theoretically simulate the rehabilitation movement of ankle joints in different patients, there are practical considerations to address. These include addressing processing and assembly errors of the robot, as well as mitigating wearing errors of both the robot and the patient. Future work should focus on adding flexible joints and components to enhance the compliance, safety, and comfort of the robot system. Additionally, studying the human-machine interaction force between the robot and the patient is essential. Furthermore, it is worth noting that the prototype proposed in this study adopts an arc-shaped sliding rail design, which may pose challenges such as machining difficulties, high accuracy requirements, and increased cost. As a potential solution, turntable bearings can be considered as a replacement for the arc-shaped sliding rails during the later stages of prototype manufacturing.

Acknowledgements
Not applicable.

Authors' Contributions
JZ was in charge of the whole research; JS wrote the manuscript; JW assisted with the analysis and validation, the remaining discussed and read the manuscript. All authors read and approved the final manuscript.

Authors' Information
Jingke Song, born in 1994, is currently a PhD candidate at *Key Laboratory of Robot Perception and Human-Machine Fusion, Hebei University of Technology, China*. His research interests include parallel mechanisms and rehabilitation robot.
Jun Wei, born in 1985, is currently a master candidate supervisor at *Key Laboratory of Robot Perception and Human-Machine Fusion, Hebei University of Technology, China*. His research interests include parallel mechanism and rehabilitation robot, and reconfigurable mechanisms.
Bin Yu, born in 1996, is currently a PhD candidate at *Key Laboratory of Robot Perception and Human-Machine Fusion, Hebei University of Technology, China*. His research interests include parallel mechanism and rehabilitation robot.
Chenglei Liu, born in 1995, is currently a PhD candidate at *Key Laboratory of Robot Perception and Human-Machine Fusion, Hebei University of Technology, China*. His research interests include parallel mechanism and rehabilitation robot.
Cunjin Ai, born in 1989, is currently a PhD candidate at *Key Laboratory of Robot Perception and Human-Machine Fusion, Hebei University of Technology, China*. His research interests include parallel mechanisms and rehabilitation robot.
Jianjun Zhang, born in 1971, is currently a professor and a PhD candidate supervisor at *Key Laboratory of Robot Perception and Human-Machine Fusion, Hebei University of Technology, China*. He received his PhD degree from *Beijing University of Aeronautics and Astronautics, China*, in 2004. His research interests include the robotic mechanics, exoskeleton robot, and rehabilitation robot.

Funding
Supported by National Natural Science Foundation of China (Grant No. 52075145), S&T Program of Hebei Province of China (Grant No. 20281805Z), Hebei Provincial Natural Science Foundation of China (Grant No. E2022202130), and Central Government Guides Basic Research Projects of Local Science and Technology Development Funds of China (Grant No. 206Z1801G).

Data availability
Some or all data, models, or code generated or used during the study are available from the corresponding author by request.

Declarations

Competing Interests
The authors declare no competing financial interests.

Received: 22 November 2022 Revised: 6 November 2023 Accepted: 12 November 2023
Published online: 19 December 2023

References

[1] X F Zeng, G L Zhu, M M Zhang, et al. Reviewing clinical effectiveness of active training strategies of platform-based ankle rehabilitation robots. *Journal of Healthcare Engineering*, 2018: 2858294.
[2] S Casco, I Fuster, R Galeano, et al. Towards an ankle neuroprosthesis for hybrid robotics: concepts and current sources for functional electrical stimulation. *2017 International Conference on Rehabilitation Robotics (ICORR)*, London, UK, July 17-20, 2017, 1660-1665.
[3] M G Alvarez-Perez, M A Garcia-Murillo, J J Cervantes-Sánchez. Robot-assisted ankle rehabilitation: A review. *Disability and Rehabilitation Assistive Technology*, 2019, 15(4): 394-408.
[4] F Alnajjar, R Zaier, S Khalid, et al. Trends and technologies in rehabilitation of foot drop: A systematic review. *Expert Review of medical devices*, 2021, 18(1): 31-46.
[5] S Rahman, R Ikeura. A novel variable impedance compact compliant ankle robot for overground gait rehabilitation and assistance. *Procedia Engineering*, 2012, 41(1): 522-531.
[6] W Meng, Q Liu, M M Zhang, et al. Robot-assisted ankle rehabilitation training on an adult with cerebral palsy: A case report. *Proceedings of the ASME 2015 International Design Engineering Technical Conferences and Computers and Information in Engineering Conference*, Boston, Massachusetts, USA, August 2–5, 2015: V009T007A006.
[7] Y M Khalid, D Gouwanda, S Parasuraman. A review on the mechanical design elements of ankle rehabilitation robot. *Proceedings of the Institution of Mechanical Engineers. Part H, Journal of Engineering in Medicine*, 2015, 229(6): 452-463.
[8] Q Meng, F G Xie, X J Liu, et al. Screw theory-based motion/force transmissibility analysis of high-speed parallel robots with articulated platforms. *Journal of Mechanisms and Robotics*, 2020, 12(4): 1-15.
[9] M Girone, G Burdea, M Bouzit, et al. A stewart platform-based system for ankle telerehabilitation. *Autonomous Robots*, 2001, 10(2): 203-212.
[10] J A Saglia, N G Tsagarakis, J S Dai, et al. Control strategies for patient-assisted training using the ankle rehabilitation robot (ARBOT). *IEEE/ASME Transactions on Mechatronics*, 2013, 18(6): 1799-1808.

[11] J S Dai, T Zhao, C Nester. Sprained ankle physiotherapy based mechanism synthesis and stiffness analysis of a robotic rehabilitation device. *Autonomous Robots*, 2004, 16(2): 207-218.
[12] G Q Liu, J L Gao, H Yue, et al. Design and kinematics analysis of parallel robots for ankle rehabilitation. *International Conference on Intelligent Robots and Systems*, Beijing, China, October 9-15, 2006, 253-258.
[13] C Z Wang, Y F Fang, S Guo, et al. Design and kinematical performance analysis of a 3-RUS/RRR redundantly actuated parallel mechanism for ankle rehabilitation. *Journal of Mechanisms and Robotics-Transacions of the ASME*, 2013, 5(4): 041003.
[14] M J Dong, Y Kong, J F Li, et al. Kinematic calibration of a parallel 2-UPS/RRR ankle rehabilitation robot. *Journal of Healthcare Engineering*, 2020: 1-12.
[15] H Choi, Y J Park, K Seo, et al. A multi-functional ankle exoskeleton for mobility enhancement of gait-impaired individuals and seniors. *IEEE Robotics & Automation Letters*, 2017, 3(1): 411-418.
[16] M B Hong, G T Kim, Y H Yoon. ACE-ankle: A novel sensorized RCM (remote-center-of-motion) ankle mechanism for military purpose exoskeleton. *Robotica*, 2019, 37(12): 2209-2228.
[17] T Essomba, L N Vu. Kinematic analysis of a new five-bar spherical decoupled mechanism with two-degrees of freedom remote center of motion. *Mechanism and Machine Theory*, 2018, 119(1): 184-197.
[18] M Malosio, S P Negri, N Pedrocchi, et al. A spherical parallel three degrees-of-freedom robot for ankle-foot neuro-rehabilitation. *2012 Annual International Conference of the IEEE Engineering in Medicine and Biology Society*, San Diego, CA, USA, 2012, 3356-3359.
[19] C L Liu, J J Zhang, Z H Ma, et al. Accurate detection mechanism synthesis and robot-assisted recognition method for ankle instantaneous motion. *Mechanism and Machine Theory*, 2022, 176(1): 105000.
[20] J J Zhang, C L Liu, T Liu, et al. Module combination based configuration synthesis and kinematic analysis of generalized spherical parallel mechanism for ankle rehabilitation. *Mechanism and Machine Theory*, 2021, 166(1): 104436.
[21] J A Saglia, N Tsagarakis, J S Dai, et al. A high-performance redundantly actuated parallel mechanism for ankle rehabilitation. *The International Journal of Robotics Research*, 2009, 28(9): 1216-1227.
[22] A H Weerasingha, A D K H Pragnathilaka, W P K Withanage, et al. C-JAE: 3 DOF robotic ankle exoskeleton with compatible joint axes. *2018 Moratuwa Engineering Research Conference (MERCon)*, Moratuwa, Sri Lanka, 2018, 270-275.
[23] J B Stiehl. Inman's joint of the ankle. 2nd ed. Williams & Wilkins, 1991.
[24] R K Beals. The joints of the ankle. *The Western Journal of Medicine*, 1977, 127(2): 183-183.
[25] A Haskell, R A Mann. Biomechanics of the foot. *Atlas of Orthoses and Assistive Devices*, 2017: 311-324.
[26] J R Jastifer, P A Gustafson. The subtalar joint: Biomechanics and functional representations in the literature. *The Foot*, 2014, 24(4): 203-209.
[27] J M Li, G K Zhang, A Muller, et al. A family of remote center of motion mechanisms based on intersecting motion planes. *Journal of Mechanical Design*, 2013, 135(9): 091009.
[28] T S Zhao, J S Dai, Z Huang. Geometric analysis of overconstrained parallel manipulators with three and four degrees of freedom. *JSME International Journal Series C-mechanical Systems Machine Elements and Manufacturing*, 2004, 45(3): 730-740.
[29] K Marlow, M Isaksson, J S Dai, et al. Motion/force transmission analysis of planar parallel mechanisms with closed-loop subchains. *Journal of Mechanisms and Robotics*, 2016, 8(4): 041019.
[30] X J Liu, X Chen, M Nahon. Motion/force constrainability analysis of lower-mobility parallel manipulators. *Journal of Mechanisms and Robotics*, 2014, 6(3): 031006.
[31] B Hu, D S Shi, T F Xie, et al. Kinematically identical manipulators derivation for the 2-RPU + UPR parallel manipulator and their constraint performance comparison. *Journal of Mechanisms and Robotics*, 2020, 12(6): 1-13.
[32] J Dul, G E Johnson. A kinematic model of the human ankle. *Journal of Biomedical Engineering*, 1985, 7(2): 137-143.
[33] S Briot, I A Bonev. Singularity analysis of zero-torsion parallel mechanisms. *2008 IEEE/RSJ International Conference on Intelligent Robots and Systems*, Nice, France, September 22-26, 2008: 1952-1957.
[34] I A Bonev, J Ryu. A new approach to orientation workspace analysis of 6-DOF parallel manipulators. *Mechanism and Machine Theory*, 2001, 36(1): 15-28.
[35] S L Delp, F C Anderson, A S Arnold, et al. OpenSim: Open-source software to create and analyze dynamic simulations of movement. *IEEE Transactions on Biomedical Engineering*, 2007, 54(11): 1940-1950.
[36] T Proietti, V Crocher, A Roby-Brami, et al. Upper-limb robotic exoskeletons for neurorehabilitation: A review on control strategies. *IEEE Reviews in Biomedical Engineering*, 2016, 9(1): 4-14.
[37] N A Bhagat, V Anusha, A Berdakh, et al. Design and optimization of an EEG-based brain machine interface (BMI) to an upper-limb exoskeleton for stroke survivors. *Front Neurosci*, 2016, 10(1): 1-17.
[38] A A Blank, J A French, A U Pehlivan, et al. Current trends in robot-assisted upper-limb stroke rehabilitation: promoting patient engagement in therapy. *Current Physical Medicine and Rehabilitation Reports*, 2014, 2(3): 184-195.